

# On the use of fire radiative power, area, and temperature estimates to characterize biomass burning via moderate to coarse spatial resolution remote sensing data in the Brazilian Amazon

Wilfrid Schroeder,<sup>1</sup> Ivan Csiszar,<sup>2</sup> Louis Giglio,<sup>3</sup> and Christopher C. Schmidt<sup>4</sup>

Received 28 December 2009; revised 3 June 2010; accepted 11 June 2010; published 10 November 2010.

[1] Spaceborne instruments provide a unique view of global vegetation fire activity many times a day. In this study, we assessed the fire characterization information provided by two major products: the Terra and Aqua MODIS Thermal Anomalies product (MOD14 and MYD14, respectively) and the Wildfire Automated Biomass Burning Algorithm (WF\_ABBA) product derived from GOES East Imager. Using higher spatial resolution imagery data from the Advanced Spaceborne Thermal Emission and Reflection Radiometer (ASTER) and Landsat Enhanced Thematic Mapper Plus (ETM+) instruments, we analyzed the characterization of subpixel fires detected by MOD14, MYD14, and WF\_ABBA over parts of Brazilian Amazonia. Our results suggest that MODIS and GOES fire radiative power (FRP) estimates derived for individual fire-pixel clusters are subject to errors due to the effects of the point spread function of those instruments (underestimation of up to 75%), improper fire background characterization (overestimation of up to 80% assuming a 10 K cold bias in background temperature), and omission of small fire lines. Detection limits were approximately 11 and 9 MW for MOD14 and MYD14, respectively, and were equivalent to 27 and 19 MW for WF\_ABBA data acquired coincidentally with MOD14 and MYD14, respectively. We found a positive correlation between FRP and percentage tree cover indicating that FRP is sensitive to biomass density. Fire area and temperature estimates derived from the application of Dozier's (1981) approach to GOES data did not agree with our reference data (i.e., ASTER and ETM+ active fire masks and in situ fire temperature data), suggesting that large and variable errors could affect the retrieval of those parameters.

**Citation:** Schroeder, W., I. Csiszar, L. Giglio, and C. C. Schmidt (2010), On the use of fire radiative power, area, and temperature estimates to characterize biomass burning via moderate to coarse spatial resolution remote sensing data in the Brazilian Amazon, *J. Geophys. Res.*, 115, D21121, doi:10.1029/2009JD013769.

## 1. Introduction

[2] Quantification of vegetation fire activity and the associated emissions from biomass burning has been approached via remote sensing and modeling techniques [Andreae *et al.*, 2004; Freitas *et al.*, 2005; Kaufman *et al.*, 1990, 1992; Reid *et al.*, 2009; Setzer and Pereira, 1991]. In both cases, satellite active-fire detection data represent one of the most important parameters for calculating source emissions. Fire alert systems also depend heavily on satellite data to monitor fire activity since in many cases this is the only form of

systematic observation available (e.g., Fire Information for Resource Management System: <http://maps.geog.umd.edu/firms/>, Advance Fire Information System: <http://afis.meraka.org.za/afis/>, Sentinel: <http://sentinel1.ga.gov.au/acres/sentinel/>, INPE (Brazilian Institute for Space Research): [http://sigma.cptec.inpe.br/queimadas/index\\_in.php](http://sigma.cptec.inpe.br/queimadas/index_in.php), among others).

[3] Biomass burning applications based on remote sensing active fire data ideally require characterization of fire properties (e.g., total radiative energy, area, temperature) to calculate emissions [Boschetti and Roy, 2009; Ellicott *et al.*, 2009; Freitas *et al.*, 2005; Ichoku *et al.*, 2008; Jordan *et al.*, 2008; Palacios-Orueta *et al.*, 2005; Reid *et al.*, 2009], demanding quality pixel data that can only be achieved by nonsaturating satellite sensors [Justice *et al.*, 2002; Kaufman *et al.*, 1998]. Fire characterization using satellite data has been attempted primarily via application of the bispectral approach to estimate fire area and temperature [Dozier, 1981] and via estimation of fire radiative power (FRP) using middle infrared data [Kaufman *et al.*, 1998; Wooster *et al.*, 2003].

[4] The application of the bispectral method can be useful to produce first guess estimates of fire area and temperature

<sup>1</sup>Earth System Science Interdisciplinary Center, University of Maryland, College Park, Maryland, USA.

<sup>2</sup>NOAA/National Environmental Satellite, Data, and Information Service Center for Satellite Applications and Research, Camp Springs, Maryland, USA.

<sup>3</sup>Science Systems and Applications Inc., Lanham, Maryland, USA.

<sup>4</sup>Cooperative Institute for Meteorological Satellite Studies, University of Wisconsin at Madison, Madison, Wisconsin, USA.

over actively burning areas occupying a subpixel sized (but nevertheless large) fraction of the pixel footprint [Dozier, 1981]. However, previous theoretical assessments have indicated that limitations with Dozier's approach can lead to large errors affecting a range of real fire conditions [Giglio and Kendall, 2001]. Specifically, the Dozier method produces poor results when the target fire temperature falls outside the 600 and 1200 K range. Meanwhile, the more recent development of FRP derived from moderate and coarse resolution instruments showed great potential for emissions modeling applications since FRP was found to be well correlated with biomass consumed in a fire [Kaufman et al., 1996; Roberts et al., 2005; Pereira et al., 2009; Wooster, 2002]. To date, validation of both approaches has been extremely limited.

[5] In this study we assessed the quality of the fire characterization data available in the 1 km spatial resolution Thermal Anomalies product [Giglio et al., 2003] derived from the Moderate Resolution Imaging Spectroradiometer (MODIS) on board the Terra and Aqua satellites (MOD14 and MYD14, respectively) and the 4 km spatial resolution Wild Fire Automated Biomass Burning Algorithm (WF\_ABBA) [Prins and Menzel, 1992] derived from the Geostationary Operational Environmental Satellite (GOES) East Imager. We based our analyses on subpixel fire information derived from 30 m imagery acquired by the Advanced Spaceborne Thermal Emission and Reflection Radiometer (ASTER), which flies on board the Terra platform along with MODIS, and Landsat Enhanced Thematic Mapper Plus (ETM+) imagery. The ASTER and ETM+ instruments provided the reference data to assess fire area estimates produced by WF\_ABBA and to substantiate FRP retrievals from MODIS and GOES. Also, data from prescribed burns conducted during three individual field campaigns were used to support our assessment of fire temperature estimates derived from the GOES data. We analyzed vegetation fires across Brazilian Amazonia, a region characterized by large biomass burning activity where satellite data represent the primary source of information for emissions models and fire managers.

## 2. Data and Methods

### 2.1. MODIS Data

[6] We used the FRP estimates available with every active fire pixel reported in the MOD14 and MYD14 fire products derived from the Terra and Aqua MODIS [Giglio et al., 2003]. The MODIS FRP retrieval is based on the relationship between the emitted fire energy and the middle infrared brightness temperature and is expressed as [Kaufman et al., 1998]:

$$\text{FRP} = 4.34 \times 10^{-19} (T_4^8 - T_{4b}^8) \text{Wm}^{-2}, \quad (1)$$

where  $T_4$  and  $T_{4b}$  are the brightness temperature estimates (K) in the 4  $\mu\text{m}$  region (i.e., band 22, although band 21 is used when band 22 becomes saturated) for the target and the background pixels, respectively. The constant in equation (1) is derived empirically for the spectral interval of MODIS channel 21–22 [Kaufman et al., 1998]. The empir-

ical derivation of equation (1) is valid for FRP retrievals of fires with flaming temperatures greater than 600 K, occupying a pixel fraction less than 0.1 [Wooster et al., 2003].

### 2.2. GOES Data

[7] GOES WF\_ABBA derivation of instantaneous fire area and temperature is based on a modified version of the Dozier bispectral method. Two simultaneous equations are solved for fire area and temperature:

$$L_4 = pB(\lambda_4, T_i) + (1 - p)B(\lambda_4, T_b) + (1 - \varepsilon_4)\tau_{4s}L_{4\text{Solar}} \quad (2)$$

$$L_{11} = pB(\lambda_{11}, T_i) + (1 - p)B(\lambda_{11}, T_b) \quad (3)$$

$L_4$  and  $L_{11}$  are the 4 and 11  $\mu\text{m}$  radiances, respectively;  $B(\lambda, T)$  is the Planck function;  $p$  is the fraction of the pixel on fire;  $T_b$  is the estimated background/nonfire brightness temperature;  $T_i$  is the average instantaneous fire temperature;  $L_{4\text{Solar}}$  is the 4  $\mu\text{m}$  reflected solar radiance;  $\tau_{4s}$  is the 4  $\mu\text{m}$  transmittance; and  $\varepsilon_4$  is the 4  $\mu\text{m}$  emissivity. Giglio and Kendall [2001] showed that under ideal conditions, the accuracy of Dozier's fire size and temperature estimates is best when the target fire temperature is 600–1200 K and the fire occupies  $P > 0.0005$  of a pixel. Fire conditions where adjacent burned area is  $\sim 50$  times larger than the active fire can warrant a threshold of  $p > 0.005$ . In this study we assessed the WF\_ABBA fire temperature and size estimates derived from full native spatial resolution GOES East imagery using the method above.

[8] Wooster et al. [2003] demonstrated that it is possible to derive physically sound FRP values by approximating Planck's radiation law using a fourth-order power law applied to middle infrared remote sensing data over the range of typical vegetation fire temperatures (i.e., 600–1500 K). After relatively simple considerations are made following the approximation above, FRP estimates can be calculated through the application of the following equation [Wooster et al., 2005]:

$$\text{FRP} = \frac{\sigma}{a} (L_{2,f} - L_{2,b})S, \quad (4)$$

where  $L_{2,f}$  and  $L_{2,b}$  are here represented by the GOES Imager channel 2 radiances ( $\text{W m}^{-2} \text{sr}^{-1} \mu\text{m}^{-1}$ ) estimated for the target pixel containing the fire and for the background pixels, respectively;  $\sigma$  is the Stefan-Boltzmann constant ( $5.67 \times 10^{-8} \text{Wm}^{-2} \text{K}^{-4}$ );  $a$  is a constant derived for the particular spectral response function of channel 2 (value for GOES-12 Imager:  $3.08 \times 10^{-9} \text{Wm}^{-2} \text{sr}^{-1} \mu\text{m}^{-1} \text{K}^{-4}$ ); and  $S$  is the ground equivalent pixel area ( $\text{m}^2$ ).

[9] Derivation of GOES FRP must take into consideration the significant along-scan pixel overlap that occurs during normal Imager operation [Menzel and Purdom, 1994]. Under such conditions, every point on the surface is effectively imaged by two adjacent pixels. Consequently, two adjacent along-scan WF\_ABBA fire pixels may be produced representing one subpixel surface fire. This condition could lead to an overestimation of GOES FRP for fires composed of two or more pixels based on (4), as the term  $S$  would be artificially increased. To deal with the uncertainties in

**Table 1.** Temperature and Duration of Flaming Stage Describing Distinct Fire Conditions

	Percentage Tree Cover	Temperature	Duration
Fire 1 (grassland)	Very low (<20%)	688 K	3 min
Fire 2 (secondary forest)	Moderate-low (≥20%, <40%)	863 K	6 min
Fire 3 (forest conversion)	Moderate-high (≥40%, <60%)	1133 K	15 min
Fire 4 (piled debris)	High (≥60%)	1153 K	>30 min

subpixel fire location and the effects of along-scan pixel overlap, we calculated GOES FRP for fire-pixel clusters containing two or more adjacent pixels in the along-scan direction by assigning variable weights to those pixels. The weighting criterion was based on the brightness temperature of each pixel; brighter pixels were assigned greater relevance in the FRP calculations. For example, for a fire composed of three adjacent pixels in the along-scan direction we calculated the GOES FRP using the following two steps:

[10] 1. Rank pixels according to their brightness temperatures (e.g.,  $T_2 > T_1 > T_3$ )

[11] 2. Assign greater weight to brighter pixels in the calculations by adjusting the pixel area in (4) using

$$\begin{aligned}
 FRP_1 &= \frac{\sigma}{a} (L_{1,f} - L_{1,b}) \times (S_1 - S_{2r1}) \\
 FRP_2 &= \frac{\sigma}{a} (L_{2,f} - L_{2,b}) \times (S_2) \\
 FRP_3 &= \frac{\sigma}{a} (L_{3,f} - L_{3,b}) \times (S_3 - S_{2r3}) \\
 FRP_{cluster} &= FRP_1 + FRP_2 + FRP_3
 \end{aligned} \quad (5)$$

where the symbols are similar to equation (4) except for  $S_{i \cap j}$ , which indicates the area of overlap between adjacent pixels  $i$  and  $j$  (i.e., the intersection of the projected pixel area on the surface calculated for adjacent pixels). Another way to deal with the GOES Imager pixel overlap is to eliminate every other adjacent fire pixel along the same scan line. We opted to use the weighting method above to preserve and take advantage of the fire signal coming from all fire pixels detected by the WF\_ABBA algorithm, in particular because of the relatively high omission error rates found for that product [Schroeder et al., 2008].

### 2.3. ASTER and ETM+ Data

[12] We used 285 ASTER and ETM+ scenes to estimate active fire areas in the Brazilian Amazonia. The scenes were distributed in the main areas of fire activity in the region and were acquired during 2001–2005. Active fire masks at 30 m spatial resolution were produced for ASTER and ETM+ data following the approach described in the studies by Giglio et al. [2008] and Schroeder et al. [2008], respectively. We did not derive fire temperature from ASTER and ETM+ data primarily due to (1) frequent saturation of active fire pixels mapped and (2) lack of a 4  $\mu\text{m}$  fire sensitive band that greatly limits the calculation of that parameter.

[13] Contiguous 30 m active fire pixels were clustered together to produce individual fire area estimates. Fire-pixel cluster area estimates derived from ASTER and ETM+

assumed that the entire footprint of a 30 m fire pixel was burning. This assumption likely result in overestimation of the fire areas produced because most of the pixels may not actually be completely on fire. Consequently, fire area estimates derived in this study using ASTER and ETM+ data should be interpreted as an upper limit for the individual fires sampled. Nevertheless, the fire area estimates produced represent the most reliable set of data currently available that can cover large geographic areas providing valuable information for numerous fire episodes.

[14] The data above were used to assess the fire area estimates produced by WF\_ABBA. We restricted the time difference separating the GOES images and the ASTER and ETM+ data used to a maximum of 15 min to reduce the effects of short term variations in fire conditions [see Csiszar and Schroeder, 2008].

### 2.4. Field Data

[15] Ground measurements of fire temperature were obtained from prescribed burns implemented during three field campaigns in Brazilian Amazonia. We used a thermo-couple linked to a data logger (Campbell Scientific Inc. CR21X) recording instantaneous temperatures at 0.2 Hz beginning at the approach of the fire lines and their passage, extending up to approximately 30 min to 1 h into the smoldering phase. Table 1 shows the average conditions describing four primary fires of interest that burned incrementally larger amounts of biomass, ranging from low to high percentage tree cover vegetation areas (see Hansen et al. [2002, 2003] for more information about the percentage tree cover data used). Additional details including the temporal progression of the different fires sampled are given by Schroeder et al. [2008].

### 2.5. Simulation of Satellite Point Spread Function (PSF) Effect on FRP Retrieval

[16] As described by the point spread function (PSF) for an optical sensor, the radiance corresponding to each pixel will be influenced by the spatial arrangement of the subpixel fire features and also radiance emanating from surface elements located just outside the pixel's nominal area [Cahoon et al., 2000; Calle et al., 2009; Zhang et al., 2006; Zhukov et al., 2006]. Previous studies provided little information on the effects of PSF on calculation of fire characteristics, in particular FRP, making this a priority area for investigation. For its size and temperature estimates calculated using Dozier's bispectral method, the WF\_ABBA product contains a correction factor to address the loss of signal in the nominal pixel footprint due to the PSF but that does not address the issue of the relative position of the fire cluster for an individual fire. The WF\_ABBA correction factor comes from analysis of the GOES PSF, which indicates that in the 4  $\mu\text{m}$  band 85% of the radiance comes from within the nominal pixel footprint [Williams et al., 1996]. The radiance is corrected by subtracting 15% of the estimated background radiance from the pixel radiance to account for leakage in from the surrounding background, and then divided by 0.85 to account for the assumed lost radiance. A similar calculation is made for the 11  $\mu\text{m}$  band, wherein 70% of the radiance is assumed to come from within the nominal pixel footprint.

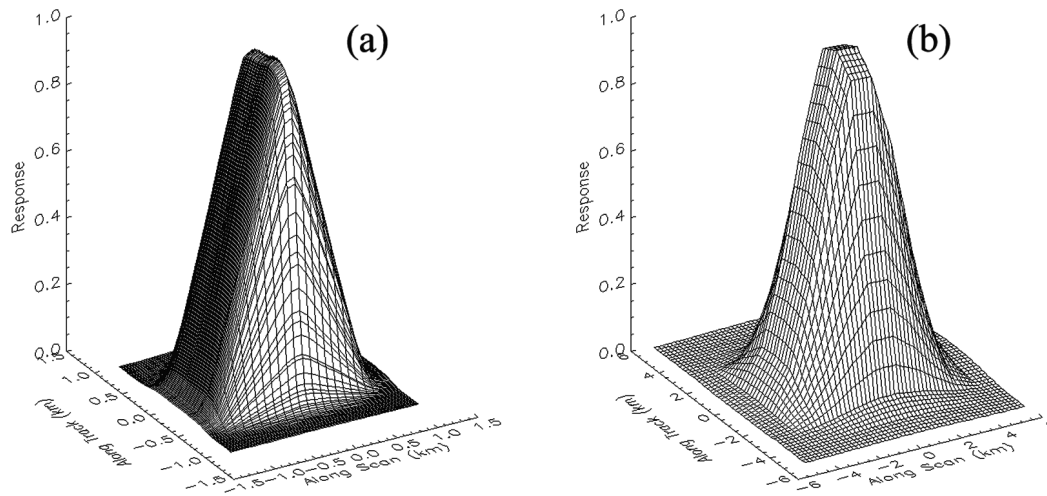


**Figure 1.** Three-dimensional representation of the point spread function of (a) MODIS and (b) GOES  $4 \mu\text{m}$  channels.

[17] Using simulation data, we assessed how the relative position of a fire contained in a moderate to coarse spatial resolution pixel affects the FRP retrieved from MODIS and GOES using equation (4). A simplified model was built assuming target pixels of nominal spatial resolution ( $1 \times 1 \text{ km}$  for MODIS and  $4 \times 4 \text{ km}$  for GOES) containing a high temperature source at  $1000 \text{ K}$  with a fixed area of approximately  $0.1 \text{ ha}$  ( $15 \times 75 \text{ m}$ ). The FRP of the fire is  $63.8 \text{ MW}$ . A uniform temperature homogeneous background composed of unburned vegetation was used in the calculations; we applied a  $300 \text{ K}$  background temperature after inspection of several different areas adjacent to active fire pixels found in the study region. The location of the fire relative to the pixel center varied in our simulations to cover half the distance separating two adjacent pixels, i.e.,  $0.5 \text{ km}$  along scan and  $0.5 \text{ km}$  along track for MODIS and  $1.25 \text{ km}$  along scan and  $2 \text{ km}$  across scan for GOES. The reduced along-scan spatial tolerance in GOES reproduces the oversampling characteristic of its Imager. The shapes of the PSF for MODIS and GOES are shown in Figures 1a and 1b, respectively. The PSF data used in this study was provided by the MODIS Characterization Support Team, whereas the GOES PSF data were provided by the Lincoln Laboratory at the Massachusetts Institute of Technology.

### 3. Results and Discussion

#### 3.1. MODIS and GOES FRP

[18] FRP estimates were produced for 12 pairs of near-coincident MODIS Terra and GOES imagery and for 11 pairs of near-coincident MODIS Aqua and GOES imagery, each containing several fire-pixel clusters. The GOES images were registered to MODIS to minimize navigation errors, and FRP values were derived for each fire-pixel cluster. Clusters with one or more saturated pixels in the middle infrared channel (approximately 3.5% of the GOES data) were not used. To ensure that individual pairs of MODIS and GOES fire-pixel clusters were representative of the same surface fire, we discarded all cases having more

than one fire cluster from each instrument within a  $10 \text{ km}$  radius.

[19] The spatially and temporally coincident FRP estimates for MODIS Terra and GOES and MODIS Aqua and GOES are shown in Figures 2a and 2b, respectively. The correlation between MODIS and GOES remained low despite all measures adopted to reduce artifact contamination of the pairs of FRP values produced; the majority of the data points in Figures 2a and 2b (77% and 75%, respectively) show a difference greater than 20% between MODIS and GOES FRP retrievals. The FRP retrievals using GOES Imager data were larger than those derived using MODIS/Terra and MODIS/Aqua data for 69% and 66% of the data points displayed in Figures 2a and 2b, respectively. Inspection of a subset of 77 pairs of MODIS Terra and GOES fire-pixel clusters using coincident ASTER data helped us identify the major factors influencing our results.

[20] First, differences in FRP were found to prevail over areas of high landscape heterogeneity. Fire pixels located in areas of marked variation in vegetation cover occurring at the same spatial scale of the MODIS or GOES pixels (e.g., deforestation sites in high percentage tree cover regions) showed systematically larger differences in FRP-based fire intensity compared to areas of homogeneous background (e.g., grasslands in low percentage tree cover regions) (Figure 3). Differences between the vegetation cover of the target pixels and their surrounding areas are expected to influence the background characterization affecting the derivation of FRP through (1) and (4) [Wooster *et al.*, 2005]. Detection clusters covering areas of deforestation where the surrounding pixels were partially or entirely covered by evergreen tropical forests were particularly prone to produce large differences between MODIS and GOES FRP values. In these cases, the brightness temperature of the closed canopy forested pixels can be as much as  $15 \text{ K}$  cooler than the true fire-pixel background, resulting in potentially large FRP overestimation especially when relatively small fires are processed. It is plausible that the resolution differences between the two sensors enhance the effect of back-

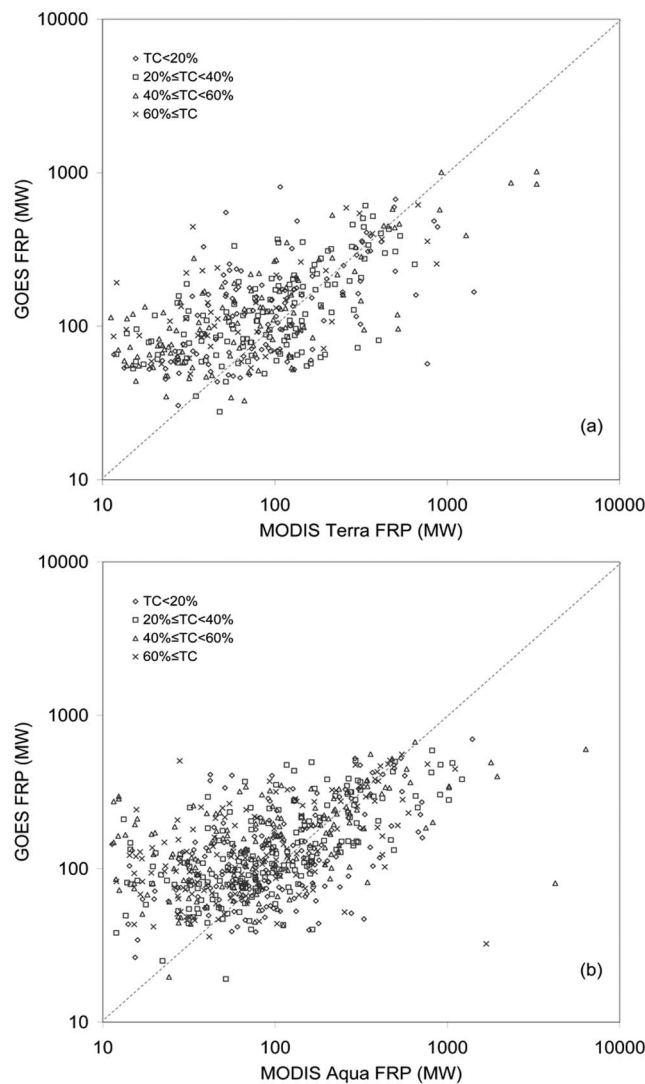


**Figure 2.** Scatterplots of FRP estimates produced for spatially and temporally coincident (a) MOD14-WF\_ABBA ( $R^2 = 0.43$ ) and (b) MYD14-WF\_ABBA ( $R^2 = 0.17$ ) fire-pixel clusters. The symbols illustrate the mean percentage tree cover (TC) based on vegetation continuous fields (VCF) data [Hansen *et al.*, 2002, 2003] for the area where the fire was located.

ground characterization in the calculation of FRP since each sensor see the scene differently. Also, the search for valid background values in GOES Imager data using  $\sim 4$  km incremental radii from the target fire pixel, compared to  $\sim 1$  km from MODIS, does in many cases, particularly near boundaries between distinct land cover types, more rapidly result in pixels of significantly different characteristics being selected to estimate the background, thereby introducing potentially larger errors in the FRP estimates.

[21] Despite the differences found between GOES and MODIS FRP estimates, results from both sensors show that FRP is sensitive to variations in biomass density as revealed by the increase in mean fire intensity with percentage tree cover (Figure 3). Short duration and low temperature fires associated with land maintenance tend to dominate in low

percentage tree cover, whereas longer duration high temperature fires typical of land conversion prevail in high percentage tree cover areas [Schroeder *et al.*, 2008]. Consequently, higher combustion rates should then be expected in densely vegetated areas resulting in larger FRP values compared to more sparsely vegetated areas. The trends in MODIS and GOES FRP values seen in Figure 3 therefore are consistent with typical vegetation fires that occur in the region analyzed.

[22] Figure 4 shows an example of a conversion fire composed of two adjacent 500 and 350 m long active lines for which one WF\_ABBA and two MOD14 fire pixels were produced. The resulting FRP estimates derived using the MODIS and GOES data showed good agreement and were equivalent to 95 and 92 MW, respectively. To illustrate the effect of background characterization in the calculation of FRP, we replaced the GOES mid-infrared pixels used to estimate the background radiance (pixels marked “X” in Figure 4; radiance values ranging from  $0.71$  to  $0.97 \text{ Wm}^{-2} \text{ sr}^{-1} \mu\text{m}^{-1}$ ) with nearby closed canopy forest equivalent radiance values ( $\sim 0.57 \text{ Wm}^{-2} \text{ sr}^{-1} \mu\text{m}^{-1}$ ; approximately 10 K cooler background) while preserving the target fire pixel radiance ( $1.07 \text{ Wm}^{-2} \text{ sr}^{-1} \mu\text{m}^{-1}$ ) unchanged. In this case, the MODIS pixels used for background characterization were assumed invariant. The MODIS background pixels were derived from a  $5 \times 5$  window centered on the fire pixel; the fire pixel itself and the two adjacent pixels along the same scan line were not considered for background characterization resulting in 22 valid background pixels in each case. The MODIS channel 22 background radiance ranged from  $0.68$  to  $1.28 \text{ Wm}^{-2} \text{ sr}^{-1} \mu\text{m}^{-1}$ , where the channel 21 radiances for the two fire pixels (channel 22 was saturated) were equal to  $3.0$  and  $3.24 \text{ Wm}^{-2} \text{ sr}^{-1} \mu\text{m}^{-1}$ . The modified GOES FRP value calculated using equation (4) increased by 82%, whereas the MODIS estimate remained constant, a signifi-

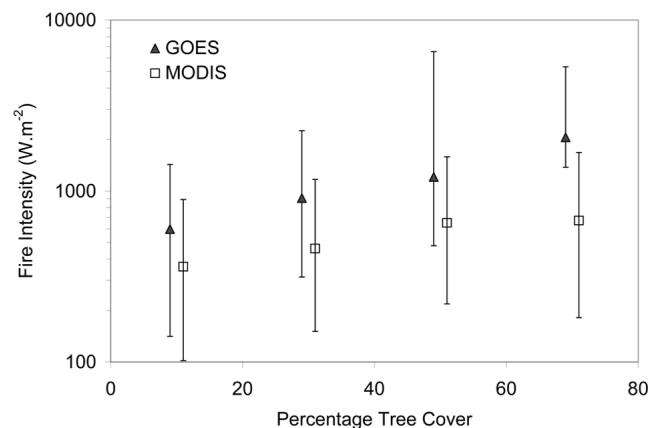


**Figure 3.** Fire intensity ( $\text{Wm}^{-2}$ ) estimates for four percentage tree cover intervals (VCF data [Hansen *et al.*, 2002, 2003]) calculated as per pixel FRP estimates for GOES and MODIS divided by the approximate active fire area determined using coincident 30 m resolution ASTER and ETM+ active fire masks (the total area of each 30 m active fire pixel is assumed to be actively burning in this case). Values plotted represent the median, the first and the third quartiles of the fire intensity data available for each VCF interval (data points are slightly offset in the x axis to avoid overlap).

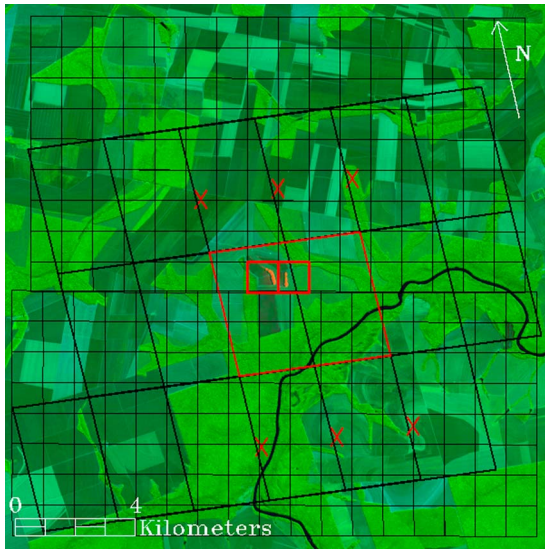


**Figure 4.** Grid depicting the pixel footprint of MODIS and GOES (shown with 50% along-scan overlap) overlaid on a near coincident ASTER scene (RGB bands 8-3-1) acquired on 27 June 2003 at 1402 UTC. Fire location: 12°16′02″S 55°42′30″W. Pixel outlines marked in red indicate MOD14 and WF\_ABBA fire pixels whereas GOES pixels marked “X” were used in the characterization of fire background. Fire lines appear as bright red and forest areas appear as vivid green; other areas are composed of deforestation and agricultural plots.

cant change that highlights the importance of landscape characteristics in the calculation of MODIS and GOES FRP through the methods described above.

[23] Differences between FRP estimates from MODIS Terra and GOES were also associated with omission of secondary fire lines contained in adjacent pixels. The landscape heterogeneity was equally important in this case as it influenced the propagation of fire lines, resulting in fragmented fires composed of several small flaming areas. Omission pixels constitute a relatively small percentage of the total energy of a fire-pixel cluster; however, their occurrence can also influence the characterization of the background pixels thereby amplifying their net effect on the FRP calculation. From the data points in Figures 2a and 2b, a detection limit of approximately 11 and 9 MW is found for the fires detected by MOD14 and MYD14, respectively, whereas WF\_ABBA detection limit corresponds to fires of approximately 27 and 19 MW for the morning (Figure 2a) and afternoon (Figure 2b) data samples, respectively.

[24] Finally, large differences between MODIS and GOES FRP values were introduced due to the effects of the PSF of each instrument. The same fires occupying the center of a pixel from one sensor and the edge of a pixel from the other sensor resulted in significantly different FRP estimates. Using the simulation data described in section 3.5, we evaluated how FRP values vary as a function of the distance of the subpixel active fire to the pixel center using the PSF information for MODIS and GOES (Figures 5a and 5b). The reduction in FRP observed when a fire is located away from the more responsive area near the pixel’s

center represented the single most important factor contributing to the differences in FRP estimates produced by MODIS and GOES. MODIS and GOES FRP estimates produced when the fire was located along the area separating two adjacent pixels represented on average 1/3 and 1/2 of their maximum value near the pixel’s center, respectively. The value used to describe the pixel area ( $S$ ) in (4) can be adjusted to best approximate the true FRP under ideal imaging condition (i.e., when the surface fire is located near the center of the pixel). In the simulations depicted in Figures 5a and 5b, we used 1 and 0.9 km<sup>2</sup> and 16 and 17.7 km<sup>2</sup> to represent the nominal and best fit pixel area values for MODIS and GOES, respectively.

[25] The predominance of relatively narrow fire lines in most biomes and the ability of MODIS Thermal Anomalies and WF\_ABBA algorithms to detect those subpixel fires can create major difficulties for the retrieval of accurate instantaneous FRP values from moderate to coarse resolution instruments. An empirical example of the sensitivity of the retrieved FRP value to the location of the fire within the pixel footprint is illustrated below. In Figure 6a, contours of four adjacent MODIS fire pixels are shown, in yellow and blue for high and nominal detection confidence, respectively, over an ASTER channels 8-3-1 (red-green-blue) image and the corresponding ASTER fire mask. Retrieved MODIS FRP values for the top two pixels are also shown. Note that the pixels on the left do not include active fires according to the ASTER fire mask. The fact that those pixels are still flagged as fire is due to the 2 km effective width of the MODIS pixel [Kaufman *et al.*, 1998; Wolfe *et al.*, 2002]; the effective pixel boundaries are shown in Figure 6b by dotted (fire pixels on the left) and dashed (fire pixels in the right) lines. Note also that in this case the fires are located in the overlap area between the two adjacent pixels, and thus, the FRP values for the two pixels represent independent retrievals for the same fires.

[26] The difference in the FRP values is caused by the different weights by which the fires are sampled in the two pixels, depending on their position within the MODIS pixel and the value of the PSF corresponding to that position. The higher FRP value corresponds to the pixel on the right where the fires are closer to the center line of the pixel.

[27] Following the formulation by Wooster *et al.* [2003], the FRP recorded by the MODIS sensor is a weighted sum of the instantaneous radiant energy according to the contribution by  $n$  thermal components within the pixel to the total radiative signal:

$$\text{FRP} = S\varepsilon\sigma \sum_{i=1}^n f_i k_i T_i^4, \quad (6)$$

where  $\varepsilon$  is emissivity,  $f_i$  is the fractional area of the  $i$ th thermal component (here the ASTER pixel), and  $k_i$  is a coefficient dependent on the location of the  $i$ th thermal component (here defined by the triangular MODIS PSF). Assuming constant  $f_i$  and uniformity of  $T_i$ , one can derive normalized FRP<sub>a</sub> values corresponding to a hypothetical rectangular-shaped PSF by

$$\text{FRP}_a = \text{FRP} \times n / \sum_{i=1}^n k_i \quad (7)$$

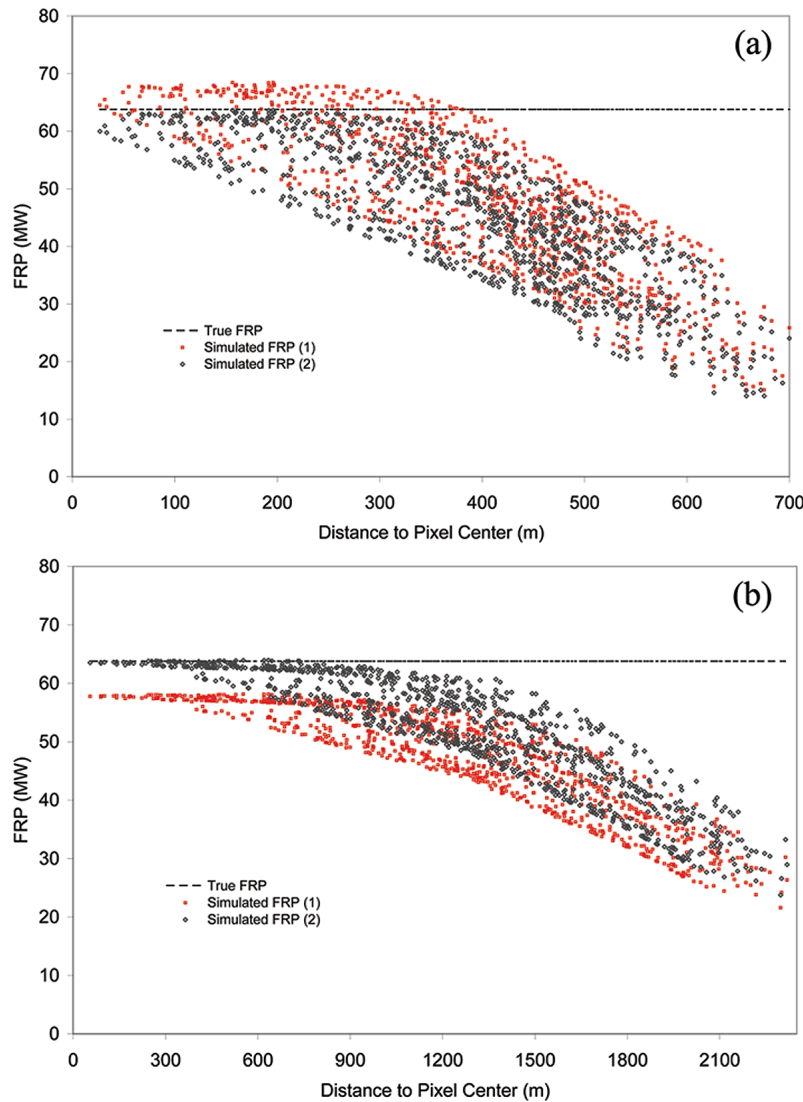


**Figure 5.** Simulated FRP for (a) MODIS and (b) GOES as a function of distance to the pixel's center. FRP estimates were calculated for a high temperature source at 1000 K covering an area of approximately 0.1 ha ( $15 \times 75 \text{ m}^2$ ). Simulated FRP (1) and (2) were calculated using 1 and 0.9 km<sup>2</sup> for the MODIS pixel area and 16 and 17.7 km<sup>2</sup> for the GOES pixel area. Dashed line represents the true FRP value (63.7 MW).

In our example the adjusted FRP<sub>a</sub> values for the two pixels examined are in close agreement (69.81 and 63.03 MW for the left and right pixels, respectively). The values are much closer than the original FRP values, demonstrating the impact of the uneven spatial sampling within the pixel, described by the PSF. The differences between the two FRP<sub>a</sub> values are primarily due to imperfect ASTER fire masks and errors caused by the assumptions of constant fractional areas and fire temperatures.

### 3.2. GOES Fire Area and Temperature Estimates

[28] Our ASTER and ETM+ reference data yielded  $N = 113$  WF\_ABBA fire pixels of nominal confidence representing an unsaturated, cloud free pixel, allowing the application of the bispectral method to retrieve fire area and

temperature estimates from the GOES data. Figure 7 shows the scatter plot depicting the pairs of fire area estimates produced by WF\_ABBA and the reference ASTER and ETM+ data. When all matchups are used, the simple analysis of correlation using the data points in Figure 7 showed a lack of correspondence between WF\_ABBA and the reference fire area estimates (coefficient of correlation  $r = -0.22$ ). As the area estimates from ASTER and ETM+ represent an upper envelope of the true actively burning areas, having data points only on and below the 1:1 line in Figure 7 (i.e., GOES area retrievals smaller than or equal to the ASTER and ETM+-based estimates) would be acceptable. However, there is a spread of the GOES fire area estimates on both sides of the 1:1 line. When the matchups are limited to those with Dozier-derived fire temperatures

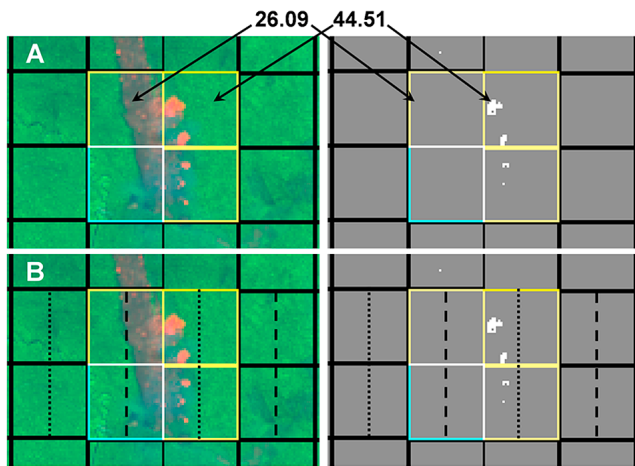


**Figure 6.** Contours of 1 km MODIS pixels over an ASTER channels (left) 8-3-1 red-green-blue image and (right) a fire mask (fires in white). The ASTER scene is from 19 August 2003 1419 UTC and is centered at 10°04'S 59°92'W. The numbers on the top are retrieved MODIS FRP values (MW). Yellow and blue MODIS contours indicate high and nominal detection confidence, respectively. The dotted and dashed lines are the true pixel boundaries.

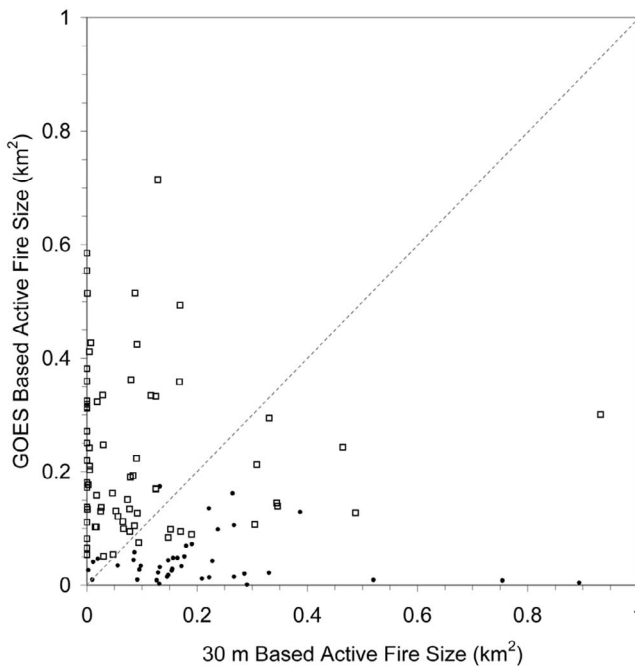


**Figure 7.** Scatterplot of fire area estimates derived independently by the WF\_ABBA algorithm (vertical axis) and from active fire masks using 30 m spatial resolution ASTER and ETM+ imagery (horizontal axis). Dots represent WF\_ABBA fire pixels with estimated fire temperature (Dozier's method) >500 K, whereas squares represent fire pixels with estimated fire temperatures <500 K.

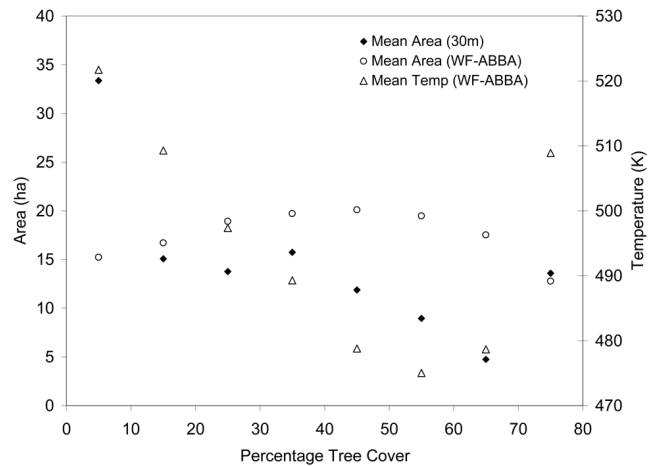


**Figure 8.** Fire area and temperature estimates derived from the WF\_ABBA product and depicted as a function of percentage tree cover. Fire area estimates derived from 30 m spatial resolution data (ASTER and ETM+) for the projected area of WF\_ABBA fire pixels are also presented.

greater than 500 K, the occurrence of data points above the 1:1 line is significantly reduced although the sample size represented in this case is relatively small ( $N = 41$ ).

[29] Fire area and temperature are known to be influenced by the regional variations in vegetation conditions and land use. *Schroeder et al.* [2008] showed that WF\_ABBA fire detection performance is sensitive to those variations resulting in lower omission errors across higher percentage tree cover areas where fires burn at higher temperatures thereby requiring less active flaming area to trigger the detection algorithm as compared to lower percentage tree cover areas. Using 4 years (2002–2005) of WF\_ABBA fire detection data from Amazonia, we assessed the consistency of the mean fire area and temperature estimates as a function of percentage tree cover data using 10% stepwise increments (Figure 8). For comparison purposes, Figure 8 also shows the mean fire area estimates derived from ASTER and ETM+ data. Those estimates were produced for the projected area coincident with approximately 460 WF\_ABBA fire pixels of various confidence levels occurring in the same period indicated above.

[30] The data points in Figure 8 suggest that (1) with the exception of those cases occurring in low percentage tree cover areas (i.e., <10%), the potential overestimation of fire areas derived from ASTER and ETM+ data showed no apparent effect on the large differences separating those estimates from the ones derived using the bispectral method applied to GOES data; (2) the smaller WF\_ABBA mean fire area values derived for percentage tree cover <40% indicate potential errors in those estimates as the lower probability of detection of WF\_ABBA associated with such vegetation requires larger fire areas compared to higher percentage tree cover pixels (where higher fire temperatures predominate hence demanding less active fire area to trigger the detection) [*Schroeder et al.*, 2008]; (3) higher temperature estimates occurring under low percentage tree cover vegetation conflicts with the fundamental assumption of higher temperature values found in more densely vegetated areas (Table 1); and (4) fire temperature estimates are predomi-

nantly low and consequently are not representative of actual flaming temperatures described in Table 1.

#### 4. Conclusions

[31] In this study we assessed the characterization of vegetation fire properties retrieved from moderate to coarse spatial resolution MODIS and GOES active fire products. Active fires of relatively small area predominated in the ASTER and ETM+ data used in our analyses. The challenges for active fire detection products based on moderate to coarse resolution data are many in this case, regardless of the algorithm used. For instance, fire characterization via FRP could show large errors depending in particular on the spatial configuration of individual active fires contained within the pixel footprint and on how the energy released by the fire is represented by the instrument's PSF. Additionally, in areas where the landscape heterogeneity is high such as some of the deforestation hot spots sampled in our study, derivation of reliable FRP values can be made difficult as a result of poor fire background characterization.

[32] In terms of fire area and temperature quantification, our results suggest that the limitations in the application of Dozier's bispectral method to GOES data prevent the consistent mapping of fire characteristics across a wide range of fire conditions. This study corroborates the results of *Giglio and Kendall* [2001] who also found large potential errors affecting fire area and temperature estimates derived using the bispectral method applied to moderate to coarse spatial resolution pixels. Fire data users must understand these limitations when applying those estimates to characterize fire conditions.

[33] The results above summarize some of the major limitations of current moderate to coarse spatial resolution satellite active fire detection products. We also found good agreement with those of *Zhukov et al.* [2006], who looked at fire characterization data using higher spatial resolution (370 m) data from the Bispectral Infrared Detection experimental satellite. Despite the limitations in fire characterization described above, increased demand for fire information is gradually leading to the sophistication of the available satellite fire detection products. Recent developments include a version of the GOES WF\_ABBA product that incorporates additional data layers as well as per pixel FRP estimates to complement the existing set of parameters describing fire area and temperature. The higher temporal resolution of that instrument provides greater capabilities for the integration of FRP over the lifetime of detected fires compared to single daytime observations typical of polar orbiting instruments. Using Spinning Enhanced Visible and Infrared Imager data over Africa, *Roberts et al.* [2005] successfully demonstrated the potential of geostationary data for FRP-based biomass burning monitoring.

[34] This study serves to illustrate the difficulty of generating an integrated fire product based on physical quantities derived from different moderate to coarse spatial resolution sensors, as estimates of quantitative fire characteristics such as FRP can be largely incompatible. The next-generation suite of sensors to become operational on board the National Polar-orbiting Operational Environmental Satellite System and the GOES-R will show improvements in spatial resolution (and temporal resolution in

the case of GOES-R) that could result in greater fire detection and characterization capabilities compared to existing products. Likewise, the Hyperspectral Infrared Imager (HypSIRI) mission that is planned to launch during the second half of this decade will provide higher spatial resolution (60 m) data including a 4  $\mu\text{m}$  band to support fire applications which, in combination with visible-near-infrared and thermal infrared bands should enable improved estimation of active fire properties and foster related pre and post fire analyses. The potential for future integration of satellite fire products should be considered in light of those new data sets. Improved data quality should create new opportunities to develop better and more detailed information about fire activity with important consequences for the understanding of regional and global climate system processes and their implications to society.

[35] **Acknowledgments.** This work was supported by NASA Headquarters under the Earth and Space Science Fellowship Program grant NNG05GP77H, NASA LBA-Eco Phase III, and EOS/NPP programs. We thank X. Xiong for providing MODIS instrument characterization data used in this study.

#### References

- Andreae, M. O., D. Rosenfeld, P. Artaxo, A. A. Costa, G. P. Frank, K. M. Longo, and M. A. F. Silva-Dias (2004), Smoking rain clouds over the Amazon, *Science*, *303*, 1337–1342, doi:10.1126/science.1092779.
- Boschetti, L., and D. P. Roy (2009), Strategies for the fusion of satellite fire radiative power with burned area data for fire radiative energy derivation, *J. Geophys. Res.*, *114*, D20302, doi:10.1029/2008JD011645.
- Cahoon, D. R., Jr., B. J. Stocks, M. E. Alexander, B. A. Baum, and J. G. Goldammer (2000), Wildland fire detection from space: Theory and application, in *Biomass Burning and its Inter-Relationships with the Climate System*, edited by J. L. Innes et al., pp. 151–169, Kluwer Acad., Dordrecht and Boston.
- Calle, A., J.-L. Casanova, and F. González-Alonso (2009), Impact of point spread function of MSG-SEVIRI on active fire detection, *Int. J. Remote Sens.*, *30*(17), 4567–4579.
- Csiszar, I., and W. Schroeder (2008), Short-term observations of the temporal development of active fires from consecutive same-day ETM+ and ASTER imagery in the Amazon: Implications for active fire product validation, *IEEE J. Selected Topics Appl. Earth Observ. Remote Sens.*, *1*(4), 248–253.
- Dozier, J. (1981), A method for satellite identification of surface temperature fields of subpixel resolution, *Remote Sens. Environ.*, *11*, 221–229.
- Ellicott, E., E. Vermote, L. Giglio, and G. Roberts (2009), Estimating biomass consumed from fire using MODIS FRE, *Geophys. Res. Lett.*, *36*, L13401, doi:10.1029/2009GL038581.
- Freitas, S. R., K. M. Longo, M. A. F. Siva-Dias, P. L. Silva-Dias, R. Chatfield, E. Prins, P. Artaxo, G. A. Grell, and F. S. Recuero (2005), Monitoring the transport of biomass burning emissions in South America, *Environ. Fluid Mech.*, *5*, 135–167.
- Giglio, L., and J. Kendall (2001), Application of the Dozier retrieval to wildfire characterization: A sensitivity analysis, *Remote Sens. Environ.*, *77*, 34–49.
- Giglio, L., J. Descloitres, C. O. Justice, and Y. Kaufman (2003), An enhanced contextual fire detection algorithm for MODIS, *Remote Sens. Environ.*, *87*, 273–282.
- Giglio, L., et al. (2008), Active fire detection and characterization with the Advanced Spaceborne Thermal Emission and Reflection Radiometer (ASTER), *Remote Sens. Environ.*, *112*(6), 3055–3063.
- Hansen, M. C., R. S. DeFries, J. R. Townshend, R. Sohlberg, C. Dimiceli, and M. Carroll (2002), Towards an operational MODIS continuous fields of percent tree cover algorithm: Examples using AVHRR and MODIS data, *Remote Sens. Environ.*, *83*, 303–319.
- Hansen, M. C., R. S. DeFries, J. R. Townshend, M. Carroll, C. Dimiceli, and R. Sohlberg (2003), Global percent tree cover at a spatial resolution of 500 meters: First results of the MODIS Vegetation Continuous Fields Algorithm, *Earth Interactions*, *7*(10), 1–15.
- Ichoku, C., L. Giglio, M. J. Wooster, and L. A. Remer (2008), Global characterization of biomass-burning patterns using satellite measurements of fire radiative energy, *Remote Sens. Environ.*, *112*(6), 2950–2962.

- Jordan, N. S., C. Ichoku, and R. M. Hoff (2008), Estimating smoke emissions over the US Southern Great Plains using MODIS fire radiative power and aerosol observations, *Atmos. Environ.*, *42*, 2007–2022.
- Justice, C., et al. (2002), The MODIS fire products, *Remote Sens. Environ.*, *83*, 244–262.
- Kaufman, Y. J., C. J. Tucker, and I. Fung (1990), Remote sensing of biomass burning in the tropics, *J. Geophys. Res.*, *95*(D7), 9927–9939, doi:10.1029/JD095iD07p09927.
- Kaufman, Y. J., A. Setzer, D. Ward, D. Tanre, B. N. Holben, P. Menzel, M. C. Pereira, and R. Rasmussen (1992), Biomass burning airborne and spaceborne experiment in the Amazonas (BASE-A), *J. Geophys. Res.*, *97*(D13), 14,581–14,599, doi:10.1029/92JD00275.
- Kaufman, Y. J., et al. (1996), Relationship between remotely sensed fire intensity and rate of emission of smoke: SCAR-C experiment, in *Biomass Burning and Global Change*, edited by J. S. Levine, pp. 685–696, MIT Press.
- Kaufman, Y. J., et al. (1998), Potential global fire monitoring from EOS-MODIS, *J. Geophys. Res.*, *103*(D24), 32,215–32,238, doi:10.1029/98JD01644.
- Menzel, W. P., and J. F. W. Purdom (1994), Introducing GOES-I: The first of a new generation of geostationary operational environmental satellites, *Bull. Am. Meteorol. Soc.*, *75*(5), 757–781.
- Palacios-Orueta, A., E. Chuvieco, A. Parra, and C. Carmona-Moreno (2005), Biomass burning emissions: A review of models using remote sensing data, *Environ. Monitor. Assess.*, *104*, 189–209.
- Pereira, G., S. R. Freitas, E. C. Moraes, N. J. Ferreira, Y. E. Shimabukuro, V. B. Rao, and K. M. Longo (2009), Estimating trace gas and aerosol emissions over South America: Relationship between fire radiative energy released and aerosol optical depth observations, *Atmos. Environ.*, *43*, 6388–6397.
- Prins, E. M., and W. P. Menzel (1992), Geostationary satellite detection of biomass burning in South America, *Int. J. Remote Sens.*, *13*, 2783–2799.
- Reid, J. S., et al. (2009), Global monitoring and forecasting of biomass-burning smoke: Description of and lessons from the Fire Locating and Modeling of Burning Emissions (Flambe) program, *IEEE J. Selected Topics Appl. Earth Observ. Remote Sens.*, *2*(3), 144–162.
- Roberts, G., M. J. Wooster, G. L. W. Perry, N. Drake, L.-M. Rebelo, and F. Dipotso (2005), Retrieval of biomass combustion rates and totals from fire radiative power observations: Application to southern Africa using geostationary SEVIRI imagery, *J. Geophys. Res.*, *110*, D21111, doi:10.1029/2005JD006018.
- Schroeder, W., E. Prins, L. Giglio, I. Csizsar, C. Schmidt, J. T. Morisette, and D. Morton (2008), Validation of GOES and MODIS active fire detection products using ASTER and ETM+ data, *Remote Sens. Environ.*, *112*(5), 2711–2726.
- Setzer, A. W., and M. C. Pereira (1991), Amazonia biomass burnings in 1987 and an estimate of their tropospheric emissions, *Ambio*, *20*(1), 19–22.
- Williams, F. L., J. C. Ehlert, and D. R. Wickholm (1996), Comparison between subsystem and system optical MTF for GOES imager, *SPIE Proc.*, *2812*(260), doi:10.1117/12.254073.
- Wolfe, R., et al. (2002), Achieving subpixel geolocation accuracy in support of MODIS land science, *Remote Sens. Environ.*, *83*, 31–49.
- Wooster, M. J., G. Roberts, and G. L. W. Perry (2005), Retrieval of biomass combustion rates and totals from fire radiative power observations: FRP derivation and calibration relationships between biomass consumption and fire radiative energy release, *J. Geophys. Res.*, *110*, D24311, doi:10.1029/2005JD006318.
- Wooster, M. (2002), Small-scale experimental testing of fire radiative energy for quantifying mass combusted in natural vegetation fires, *Geophys. Res. Lett.*, *29*(21), 2027, doi:10.1029/2002GL015487.
- Wooster, M. J., B. Zhukov, and D. Oertel (2003), Fire radiative energy for quantitative study of biomass burning: Derivation from the BIRD experimental satellite and comparison to MODIS fire products, *Remote Sens. Environ.*, *86*, 83–107.
- Zhang, P., J. Li, E. Olson, T. J. Schmidt, J. Li, and W. P. Menzel (2006), Impact of point spread function on infrared radiances from geostationary satellites, *IEEE Trans. Geosci. Remote Sens.*, *44*(8), 2176–2183.
- Zhukov, B., E. Lorenz, D. Oertel, M. Wooster, and G. Roberts (2006), Spaceborne detection and characterization of fires during the Bispectral Infrared Detection (BIRD) experimental satellite mission (2001–2004), *Remote Sens. Environ.*, *100*, 29–51.
- I. Csizsar, NOAA/National Environmental Satellite, Data, and Information Service Center for Satellite Applications and Research, Camp Springs, MD 20746, USA.
- L. Giglio, Science Systems and Applications Inc., Lanham, MD 20706, USA.
- W. Schroeder, Earth System Science Interdisciplinary Center, University of Maryland, College Park, MD 20740, USA. (wilfrid.schroeder@noaa.gov)
- C. C. Schmidt, Cooperative Institute for Meteorological Satellite Studies, University of Wisconsin at Madison, Madison, WI 53706, USA.